The computed width is $75c/\omega_{pe}$. Thus the small amount of resistive ion heating plays a crucial role in determining shock structure.

For the computation shown in Fig. 1, the Rankine-Huginiot conditions are satisfied with small fluctuations about the downstream state, and the preheating of electrons in the early phase of the shock is clearly demonstrated. The value of T_e/T_i averages about 9.5, nearly the value predicted. Furthermore, at no point in the shock is $V_{ey} > (T/m)^{1/2}$, so the electron-ion two-stream instability plays no role anywhere in the shock unless upstream, $T_i \gtrsim T_e/2.5$. Finally, notice that the value of $\langle (e\,\delta\varphi/T)^2 \rangle$ is quite close to the predicted value of 0.004.

[1]J. W. M. Paul, C. C. Daughney, and L. S. Holmes, Phys. Rev. Lett. 25, 497 (1970).

[2]P. Bogen, K. J. Dietz, K. H. Dipple, E. Hintz, K. Hothker, F. Siemsen, and G. Zeyer, in Proceedings of the Fourth Conference on Plasma Physics and Controlled Nuclear Fusion Research, Madison, Wisconsin, 1971 (to be published), Paper No. CN-28/J-11.

[3]N. A. Krall and D. L. Book, Phys. Fluids 12, 347 (1969).

[4]R. Z. Sagdeev, in *Proceedings of Symposia in Applied Mathematics*, edited by H. Grad (American Mathematical Soceity, Providence, R. I., 1967), Vol. 18, p. 281.

[5]H. V. Wong, Phys. Fluids 13, 757 (1970).

[6]D. W. Forslund, R. L. Morse, C. W. Nielson, Phys. Rev. Lett. 25, 1266 (1970).

[7]M. Lampe, W. M. Manheimer, J. B. McBride, J. H. Orens, R. Shanny, and R. N. Sudan, Phys. Rev. Lett. 26, 1221 (1971).

[8]T. P. Coffey, Phys. Fluids 13, 1249 (1970).

[9]J. P. Doherty, J. Plasma Phys. 4, 761 (1970).

[10]The expression for the growth rate given in Eq. (9) is derived under the assumption that the ions are Maxwellian. It is not necessary to make this assumption, and one could choose other models for the ion distribution function. For instance, we could easily redo the calculation assuming the ions are warm but have a hot tail.

[11]J. Adlam and J. Allen, Phil. Mag. 3, 448 (1958).

[12]J. Boris and N. Winsor, Princeton Plasma Physics Laboratory Report No. Matt-652, 1970 (unpublished).

High-Order Wave Mixing in Beam-Plasma Instabilities*

W. Carr, D. Boyd, H. Liu, G. Schmidt, and M. Seidl
Stevens Institute of Technology, Hoboken, New Jersey 07030
(Received 13 January 1972)

When two waves, ω_1 and $\omega_1+\Delta\omega$, are externally driven in an unstable beam-plasma system, they are found to couple in the nonlinear regime to produce up to ten waves, with frequencies given by $\omega_1 \pm n\Delta\omega$ and amplitudes comparable to the driver amplitudes. This situation is described in terms of third- and higher-order wave-interaction processes. It is suggested that this phenomenon is responsible for nonlinear broadening of the amplified noise spectrum.

We report on the observation of large-amplitude high-order wave interactions between high-frequency electron waves ($\omega > \omega_{ce}$) in a beam-plasma system. When two unstable waves with frequencies ω_1 and ω_2 are driven in the system, satellite waves with frequencies $\omega_n = \omega_{1,2} \pm n\Delta\omega$ are observed, where $\Delta\omega = \omega_1 - \omega_2$ and n is an integer. These satellite waves themselves are (or are close to) eigenmodes of the system, driven by the primary waves via higher-order processes. It is suggested that in the absence of driven waves the same process is responsible for the nonlinear broadening of the noise spectrum.

High-order satellites were also observed by Sato[1] in ion acoustic waves and by Chang, Raether, and Tanaka in beam-plasma waves, as a result of remixing of resonant second-order processes. In the present case the second-order process is nonresonant, but high-order satellite production is resonant and is an important process in the nonlinear regime.

The experiments were done in a hot-cathode dc discharge of diameter 3 cm in a uniform magnetic field in He at 5×10^{-4} Torr. A small electron gun producing a 500-eV beam of diameter 6 mm was placed in the plasma on axis and aligned with the magnetic field. The interaction region has a useful length of 50 cm, where axial density variation is less than 5%. Typical experimental parameters are as follows: electron cyclotron frequency $f_{ce} = 0.5$ GHz, electron plasma frequency $f_p = 0.8$ GHz, and normalized beam density $n_b/n_p = \omega_p^2/\omega_p^2 = 1\times10^{-2}$. Under these conditions

convectively unstable waves are found in a frequency band above f_{ce}, called the H^0 mode by Seidl.[3] The frequency range is $f = (0.55\text{–}0.85) \times 10^9\ \text{sec}^{-1}$ with wavelengths $\lambda = 1.4\text{–}2.3$ cm. The waves are essentially confined to the electron beam in the transverse direction.

The wave observations are made with two coaxial rf probes with diameters much smaller than a wavelength. One probe is placed in the beam near the electron gun and serves as a transmitter. The second probe is driven axially along the beam to observe the wave amplitudes. The output of the receiver probe is detected with a wide dispersion spectrum analyzer with a logarithmic output. Using the spectrum-analyzer outputs together with the receiver-probe position readout, X-Y plots are made of log$E$ versus axial distance and log$E$ versus frequency.

The nonlinear satellite generation process is very strong and is easily observed when any two unstable waves are simultaneously present in the system. A clear illustration is obtained when two waves are launched from the transmitter probe, as shown in Fig. 1. Here waves of frequencies $f_1 = 0.90$ GHz and $f_2 = 0.86$ GHz are launched with sufficient initial amplitude such that they grow and saturate before the amplified noise reaches appreciable level. In Fig. 1 the z dependence of the various waves is given. The capacitive probe coupling decays within a few centimeters and subsequently the two plasma waves grow, in agreement with linear theory. The growth here is exponential as shown by the straight portion on the semilog plot. At $z \cong 25$ cm the nonlinear effects set in simultaneously. The growth rates of both waves begin to decrease and the satellites appear. In the region $25 < z < 35$ cm there is a transition from the linear picture to the fully developed nonlinear picture. For

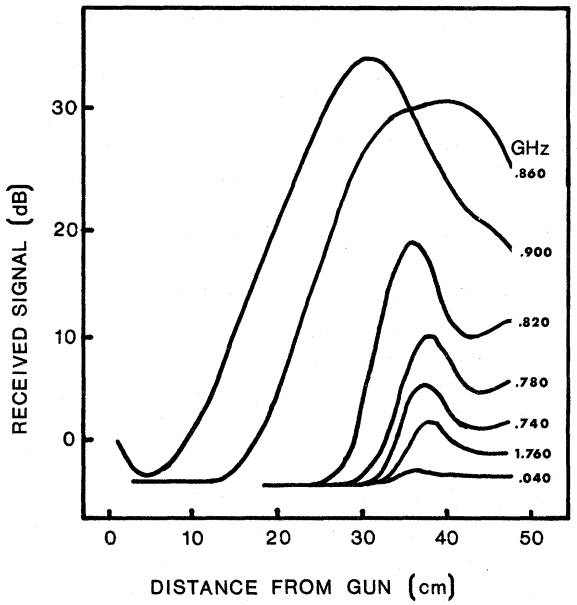

FIG. 1. Received amplitudes versus axial distance as measured from the electron gun. The driver waves are at 0.86 and 0.90 GHz, lower satellites at 0.82, 0.78, and 0.74 GHz, and sum and difference frequencies at 1.76 and 0.04 GHz, respectively. Upper satellites are not shown here.

$z > 35$ cm the evolution is complete and the wave-amplitude ratios become approximately constant. In addition to the sidebands, the received signal at the sum and difference frequencies are shown, demonstrating that the electric fields at these frequencies are small. The properties of the waves in the linear regime, $z < 25$ cm, have been studied and will be given in a separate article. The waves are found to behave according to the dispersion relation given by

$$\epsilon(\vec{k}, \omega) = 1 + \kappa_p + \kappa_b = 0, \tag{1}$$

with

$$\kappa_p = \frac{2\omega_p^2}{(k_\perp^2 + k_z^2) v_t^2}\left[1 + \frac{\omega}{|k_z| v_t} \sum_{n=-\infty}^{+\infty} Z\left(\frac{\omega - n\omega_c}{|k_z| v_t}\right) e^{-\lambda} I_n(\lambda)\right], \quad \kappa_b = -\frac{\omega_b^2}{(\omega - k_z V)^2} \frac{k_z^2}{k_\perp^2 + k_z^2},$$

where v_t is the plasma electron thermal velocity, $\lambda = (k_\perp^2 v_t^2)/2\omega_c^2$, Z is the plasma dispersion function, V is the electron beam velocity, and I_n is an nth-order modified Bessel function.

This corresponds to a warm infinite plasma in a uniform magnetic field with a weak cylindrical beam parallel to $\vec{B}$, in the electrostatic approximation; $k_\perp$ is the transverse wave number determined by the beam radius. The solution of Eq. (1) for the experimental parameters gives spatially growing waves in a frequency band above ω_{ce}, corresponding to the observed waves. The phase velocity in the band is essentially constant and is a few percent smaller than the electron beam velocity.

In the transition region, $25 < z < 35$ cm in Fig. 1, no analysis has been made for reasons of complexity. However, for $z > 35$ cm the nonlinear waves may be approximated by propagating waves. Here a simple description may be given in terms of higher-order decay processes. Expanding the distribution

function and electric field gives for the nth order

$$\frac{d}{dt}f_n+\frac{q}{m}\vec{E}_n\cdot\frac{\partial f_0}{\partial\vec{v}}=-\sum_j\frac{q}{m}\vec{E}_{n-j}\cdot\frac{\partial}{\partial\vec{v}}f_j,\quad \nabla\cdot\vec{E}_j=4\pi q\int f_j\,d^3v, \tag{2}$$

where d/dt designates differentiation along the unperturbed trajectory. Considering plane electrostatic waves one finds to lowest order the linear solution given by

$$E_1\left(1-\frac{iq^2 4\pi}{mk^2}\int d^3v\int^t\vec{k}\cdot\frac{\partial f_0}{\partial\vec{v}'(t')}\exp i\{-\omega_\alpha(t'-t)+\vec{k}_\alpha\cdot[\vec{x}'(t')-\vec{x}]\}\,dt'\right)=E_1\epsilon(\omega_\alpha,\vec{k}_\alpha)=0, \tag{3}$$

where $\vec{x}'(t')$ and $\vec{v}'(t')$ are the particle position and velocity along the unperturbed trajectory at time t', and ϵ is the linear dielectric function given by (1).

In nth order one finds from (2)

$$E_n(\omega_\sigma,\vec{k}_\sigma)=[i4\pi q^2/mk_\sigma\epsilon(\omega_\sigma,\vec{k}_\sigma)]\textstyle\sum_j\int d^3v\int^t dt'\,\vec{E}_{n-j}\cdot(\partial f_j/\partial\vec{v})\exp i\{-\omega_\sigma(t'-t)+\vec{k}_\sigma[\vec{x}'(t')-\vec{x}]\}, \tag{4}$$

where if $\vec{E}_{n-j}$ varies with $(\omega_\alpha,\vec{k}_\alpha)$ and f_j with $(\omega_\beta,\vec{k}_\beta)$, then $\omega_\alpha+\omega_\beta=\omega_\sigma$; $\vec{k}_\alpha+\vec{k}_\beta=\vec{k}_\sigma$.

In our case, waves with frequencies $\pm\omega_1$ and $\pm\omega_2$ are externally excited. The corresponding $\pm\vec{k}_1$ and $\pm\vec{k}_2$ to the lowest order satisfy the first-order dispersion relation. These waves drive second-order waves $(\pm 2\omega_{1,2},\pm 2\vec{k}_{1,2})$ and $\pm(\omega_1\pm\omega_2,\vec{k}_1\pm\vec{k}_2)$. None of these are eigenmodes of the system; the corresponding ϵ's are large, so by Eq. (4) these modes are only weakly excited. Some third-order waves, however, are close to solutions of $\epsilon=0$. For instance $\epsilon(2\omega_1-\omega_2,2\vec{k}_1-\vec{k}_2)$ and $\epsilon(2\omega_2-\omega_1,2\vec{k}_2-\vec{k}_1)$ are nearly zero, since $2\omega_1-\omega_2$ and $2\omega_2-\omega_1$ are near ω_1 and ω_2 and in this region the solution of Eq. (1) is $\omega\simeq kV$. So by Eq. (4) the corresponding waves should be strongly excited, giving rise to the first upper and lower satellites. Further satellites are generated in a similar fashion with lower-order satellites acting as drivers.

One also notes that, according to (4), $E(\omega_i+\omega_j)$ is proportional to $E(\omega_i)E(\omega_j)$. Consequently the lower-satellite amplitude $E(2\omega_2-\omega_1)$ should be proportional to $E^2(\omega_2)E(\omega_1)$, and the upper-satellite $E(2\omega_1-\omega_2)$ should be proportional to $E(\omega_2)\times E^2(\omega_1)$. This is experimentally verified in Fig. 2 where the observed amplitudes $E(2\omega_2-\omega_1)$ and $E(2\omega_1-\omega_2)$ are plotted versus $E(\omega_1)$. The log-log curve for the upper satellite has slope 2, while the lower has slope 1, in agreement with theory.

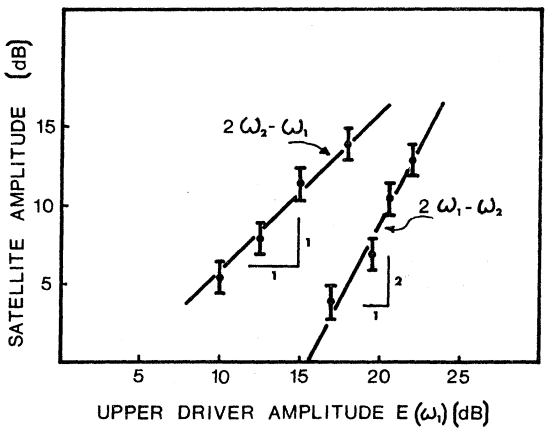

FIG. 2. Upper-satellite amplitude $E(2\omega_1-\omega_2)$, and lower-satellite amplitude $E(2\omega_2-\omega_1)$ versus upper-driver amplitude $E(\omega_1)$ with lower-driver $E(\omega_2)$ held constant.

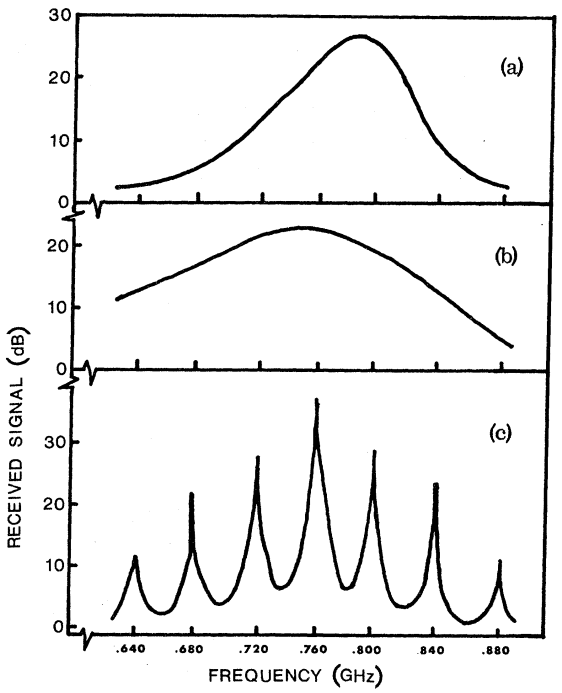

FIG. 3. Received amplitude versus frequency. (a) Instability noise spectrum in linear regime; (b) noise spectrum in nonlinear regime; (c) satellite spectrum in nonlinear regime resulting from driver waves at 0.760 and 0.800 GHz.

In the absence of external modulation, a narrow-band instability spectrum is observed corresponding to spatially amplified plasma fluctuations. In the linear regime the spectral width remains approximately constant. This linear spectrum is given in Fig. 3(a). Well into the nonlinear regime the spectrum broadens considerably, as shown in Fig. 3(b). It is suggested that high-order satellite production is responsible for this broadening, with the various components of the spectrum interacting to produce a spectrum of satellites corresponding to the wings.

A qualitative comparison of the noise broadening to the two-wave case may be obtained by simulating the linear noise spectrum by launching the two waves at the noise frequency with a separation corresponding to the spectral width. The resulting nonlinear wave spectrum corresponding to this simulation is shown in Fig. 3(c). The envelope of Fig. 3(c) has a shape much like Fig. 3(b) indicating that the satellite process generates the noise broadening.

The satellite generation process is found to be a dominant nonlinear process whenever two or more unstable waves are present in the system. The two conditions essential to this process are the constant phase velocity of the waves, resulting in resonant coupling to the satellite, and the growth of linear waves, resulting in large-amplitude driver waves. Satellite production should be an important nonlinear process whenever these two conditions are satisfied, for example, for ion acoustic instabilities.

*Work supported in part by the National Science Foundation, the U. S. Air Force Office of Scientific Research, and the U. S. Atomic Energy Commission.

[1]N. Sato, Phys. Fluids 13, 2198 (1970).

[2]J. Chang, M. Raether, and S. Tanaka, Phys. Rev. Lett. 27, 1263 (1971).

[3]M. Seidl, Phys. Fluids 13, 966 (1970).

Relation between Phonon Structure and Phase Transition in $NaClO_3$†

A. D. Prasad Rao, R. S. Katiyar, and S. P. S. Porto

Departments of Physics and Electrical Engineering, University of Southern California, Los Angeles, California 90007

(Received 17 January 1972)

Single crystals of $NaClO_3$ have been investigated to understand their ferroelectric behavior. Our investigations show that a number of transverse optic modes in the low-frequency region vary in frequency as the transition temperature is approached. The product of the squares of the frequencies of these modes varies as $T - T_c$ with $T_c \approx 576$°K. This may be a general description of Cochran's soft-mode theory in which the lowest optic mode has all the temperature dependence.

Ferroelectric behavior in crystals is explained by Cochran[1] as the result of the instability of a low-frequency normal mode at the transition temperature. Such a normal mode produces the dipole moment along the ferroelectric axis, and its temperature dependence in the paraelectric phase is given by $\omega_T^2 \propto T - T_c$, where T_c is the Curie temperature. Our observations on sodium chlorate, sodium nitrite, and sodium nitrate, however, indicate that there are several temperature-dependent modes in the low-frequency region of the Raman spectrum and none of them have the temperature dependence expressed by the above equation. Here we report the results on sodium chlorate.

$NaClO_3$ is cubic, belonging to T^4 ($P2_13$), and has four formula units in the primitive cell.[2] The temperature dependence of its static dielectric constant is typical of that of a ferroelectric with an extrapolated Curie temperature $T = 593$°K.[3] But, the melting temperature of the crystal is 537°K which makes it difficult to reach the ferroelectric transition point. The Raman spectrum of $NaClO_3$ has been studied by several workers.[4-8] Gorelik *et al.*[8] have also studied its temperature dependence up to 483°K. However, in interpreting their data they have isolated the temperature dependence of the mode at 186 cm^{-1}, and as a result they could not draw any definite conclusions from their work. In order to relate the dielectric behavior with the lattice vibration, we have reinvestigated its Raman spectrum at room temperature and followed it through the melting of the crystal. It is convenient to separate the